INSTITUTE OF PHYSICS PUBLISHING PHYSICS IN MEDICINE AND BIOLOGY

Phys. Med. Biol. **47** (2002) 4079–4092 PII: S0031-9155(02)37207-5

Three-dimensional localization of fluorescent masses deeply embedded in tissue

A Eidsath[1], V Chernomordik[2], A Gandjbakhche[2], P Smith[1] and A Russo[3]

[1] ORS/DBEPS, National Institutes of Health, Bethesda, MD 20892, USA
[2] NICHD, National Institutes of Health, Bethesda, MD 20892, USA
[3] NCI/ROB, National Institutes of Health, Bethesda, MD 20892, USA

E-mail: vchern@helix.nih.gov

Received 21 May 2002, in final form 24 September 2002
Published 30 October 2002
Online at stacks.iop.org/PMB/47/4079

Abstract

In this paper we present preliminary results obtained for tissue-like phantoms and *ex vivo* tissue slabs using a prototype system for CW infrared fluorescence imaging of fluorescent markers. Besides the design of the experimental system itself, we have developed a theoretical model of photon migration under experimental conditions and associated 3D reconstruction algorithms to estimate the distribution of fluorescent markers. Application of the developed algorithms in the analysis of 2D intensity distributions of the fluorescent light demonstrated their ability to reconstruct positions of the markers (including their depths) with good accuracy (error $\leqslant 10\%$) both for the Intralipid phantoms and *ex vivo* tissue slabs.

1. Introduction

Spectral imaging techniques using visible and near-infrared radiation have been investigated for their potential to discriminate abnormal regions (e.g., tumours) from healthy background tissues. One approach to non-invasive 'optical biopsy' widely discussed in the literature (see e.g. the recent reviews by Wagnieres *et al* (1998), Hawrysz and Sevick-Muraca (2000), Patterson and Pogue (1994), Li *et al* (1996), Gandjbakhche and Gannot (1996), Reynolds *et al* (1999), Roy and Sevick-Muraca (2001)) involves application of exogenous fluorescent markers to provide quantitative analysis of deeply embedded tissue regions. Near-infrared imaging of exogenous fluorescent contrast agents within tissue-simulating phantoms and actual tissues was presented recently (Reynolds *et al* 1999). Various image reconstruction algorithms were suggested to investigate distributions of the fluorophore inside a turbid tissue-like medium. Most of them used a diffusion approximation as a forward model to describe photon propagation in diffuse media. The initial theoretical work for this approach was done by Patterson and Pogue (1994), and used subsequently by other researchers (e.g. Li *et al* (1996)). Several recent studies got encouraging results for the image reconstruction,

using numerically simulated data in the frequency domain (Roy and Sevick-Muraca 2001, Eppstein *et al* 2001, Lee and Sevick-Muraca 2002). The transition to image reconstruction based on real experimental data provides a great challenge, and, up to now, only preliminary results using frequency-domain experimental data from basic tissue-like phantoms with a single relatively large inclusion are available (Lee and Sevick-Muraca 2002, Hawrysz *et al* 2001). The position and size of this single inclusion were reconstructed quite accurately, though the reconstructed value of the absorption coefficient was underestimated by 80% (Lee and Sevick-Muraca 2002). In a recent paper, Ntziachristos and Weissleder (2001) suggested a 3D reconstruction scheme using a Born approximation to a diffusion model as a forward model. It allowed effective 3D reconstruction of the fluorescent objects (two small cylinders embedded in a turbid medium) with good accuracy. It should be noted that another general feature of the approaches (Roy and Sevick-Muraca 2001, Eppstein *et al* 2001, Lee and Sevick-Muraca 2002, Hawrysz *et al* 2001, Ntziachristos and Weissleder 2001)—besides the forward model based on a diffusion approximation—is the experimental set-up, which implies use of multiple sources and detectors surrounding a phantom or a region of interest. Such a set-up cannot be realized in several practically important cases, which considerably limits the possible applications for this methodology.

An alternative approach to fluorescent optical biopsy that can be useful for several applications was suggested by Gandjbakhche and Gannot (1996), Gandjbakhche *et al* (1997) and Chernomordik *et al* (1999). The authors use random walk theory as a forward model for the image reconstruction and work in the reflection CW mode, using a single source and a CCD camera as a matrix detector.

It should be noted that clinically practical fluorescence imaging techniques must meet several requirements. First, the pathology under investigation must not lie at a depth where the attenuation of the signal gives poor signal-to-noise ratio and resolvability. Secondly, the specificity of the chosen fluorescent marker must be high enough so that one can clearly distinguish between the normal and abnormal regions. Finally, one must have a robust image reconstruction algorithm that enables quantification of positions and relative strengths of the fluorophores.

A promising area to use near-infrared fluorescence-based 'optical biopsy' is detecting sentinel nodes in cancer patients (see e.g. Reynolds *et al* (1999)). Lymphatic channels draining a primary tumour bed are a primary means by which tumour spread through the body. Although the sentinel node is usually defined as the first lymph node within the lymphatic channel (Hawley *et al* 1997a, Cox *et al* 2000), it is important to note that there may be more than one sentinel node per tumour bed. Anatomical predictions of lymph node basins are often wrong due to the multiplicity and variability of drainage patterns. The rationale for sentinel detection instead of total node exenteration is premised on the natural history of tumour spread—most commonly in an ordered progression from the primary site to the closest nodes and beyond (van Dongen *et al* 2000). Furthermore, when a sentinel node(s) is retrieved a more detailed analysis of one or two nodes rather than 10–40 nodes offers far greater diagnostic accuracy. Therefore, if the sentinel node can be localized and harvested, and it is shown not to have cancer cells present, then total node dissection with its attendant morbidity is obviated. When breast cancer is diagnosed, determining whether there are tumour cells within the lymph nodes has extremely important prognostic and therapeutic implications. The potential scope of optical biopsying can be appreciated when it is realized that 186 000 cases of breast cancer are diagnosed each year in the USA. Lymphoscintigraphy is often used by clinicians now for lymphatic mapping. The method provides 2D imaging of the lymphatic channels after injection of a radioactive material (Tc-99m sulfur colloid) using a standard large field-of-view gamma camera (see e.g. Glass *et al* (1999)). An inherent limitation of lymphoscintigraphy, however,

is its poor visualization of the deep lymphatic system. Moreover, the use of radioactive particles for the imaging involves important dosimetry requirements to avoid health hazards. Fluorescence based 'optical biopsy' may be a promising alternative to lymphoscintigraphy. To meet the aforementioned specificity requirements in the localization of sentinel nodes, we need a fluorescent probe that optimizes uptake into the lymphatic system. This is accomplished by modification of the size and surface properties of the probe. The excitation and emission wavelengths are also critical. The near-infrared wavelengths are ideal since there is little absorption either by haemoglobin or by water. The lymphatic drainage brings the fluorescent particles to the corresponding sentinel node in which they accumulate. Then fluorescence signal should be quantified by surface optical imaging to estimate the position of the sentinel node contiguous with the tumour. The major problem with such quantification is the highly scattering nature of the biological tissues in this spectral range. Multiple scattering results in the dispersion of the photon path lengths, loss of localization and resolution. Instead of geometrical optics, more complicated diffusion-like models of photon migration should be developed to analyse the experimental data. The methodology, presented below, allowed us to get quite an accurate 3D localization of the fluorophores that were embedded in both tissue-like phantoms and *ex vivo* tissue slabs. It enhances the potential of the corresponding diagnostics compared to the 2D localization of the fluorophores that was demonstrated in Reynolds *et al* (1999) in an analogous experimental geometry (reflection mode).

The maximum fluorophore depth of 12 mm realized in our experiments is not a physical limit of the method. In fact, the good accuracy of fluorophore localization at a depth of 12 mm implies that the system can operate for considerably deeper targets since the theoretical model (random walk) provides a better description for deeper inclusions in the turbid medium (due to larger number of photon scatterings). Projected integration times of less than a minute for depths up to several centimetres are still quite reasonable from the clinical point of view (see section 2 below).

It is worth noting that due to similarities in methods and instrumentation, our approach to localization of the embedded fluorophores, discussed in this paper, can be transferred and with some modifications employed also in the rapidly developing field of *in vivo* optical molecular imaging (for a recent review of the field see Weissleder (2002)).

2. Experimental setup

The experimental setup is shown in figure 1. The major components are a laser diode (690 nm Hitachi 40 mW controlled to ± 0.1 C using Thorlabs models LDC500 and TEC2000), a filter cube (Chroma 690/80X, 740D, 790/95E) and a cooled CCD camera (Roper Scientific—the camera is currently called the VersaArray: 512B—a 512×512 pixel back-illuminated chip with 16 bit resolution). The ability of the filter to block the scattered primary beam is critical to the success of the experiment. The emission filter has an optical density (OD) greater than 6 at 690 nm (which is the maximum that Chroma's instrumentation can measure—theoretically it is OD 9), and the dichroic is OD 3 at that wavelength. The cube thus has an OD > 9 at the excitation wavelength. The system operates in CW mode to produce a 2D fluorescent image, which through a f 1.2 Nikon lens gave a viewing area of 50×50 mm. The laser diode was collimated using an aspheric lens, and the beam was focused to approximately a 100 μm spot (a single pixel) using a 1 inch plano/convex lens. It is important to consider the integration times that are required to provide a reasonable signal-to-noise ratio to evaluate the potential of the system for the clinical applications. Since the output of the laser was held constant at 2.0 mW (measured using a Newport 1825-C power meter with 818-ST detector), deeper

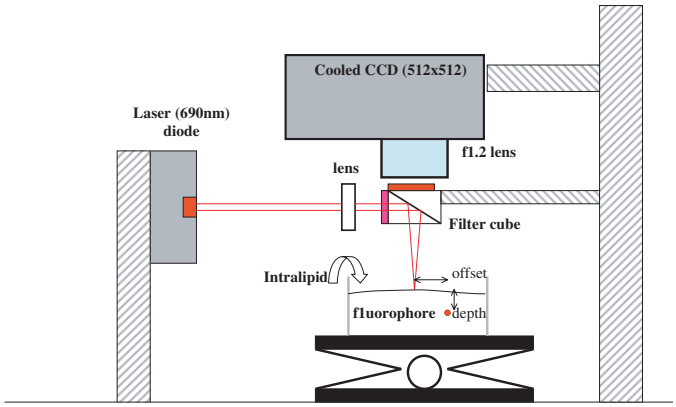

Figure 1. Experimental setup for measurements of 2D fluorescent intensity distributions.

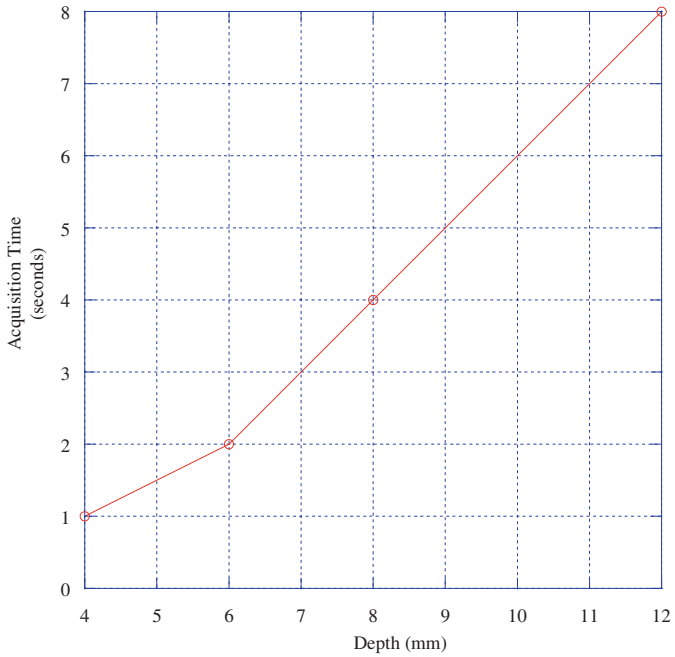

Figure 2. Acquisition time as a function of depth.

phantoms required longer integration times of the camera. Therefore, the integration time of the camera was adjusted with depth in an attempt to make use of the full 16 bits of the chip. Figure 2 shows integration time as a function of the fluorophore depth. These acquisition times vary between 1 s at the depth of 4 mm and 8 s at 12 mm. It should be noted that these values do not correspond to physical limitations of the suggested set-up. In particular, these times could have been reduced significantly by binning the CCD chip (reducing the number of pixels forming the image). We found that the results of the target localization by our algorithm vary negligibly if we reduce the total number of pixels from 512 $\times$ 512 to 128 $\times$ 128 by averaging the data from 16 (4 $\times$ 4) neighbouring pixels.

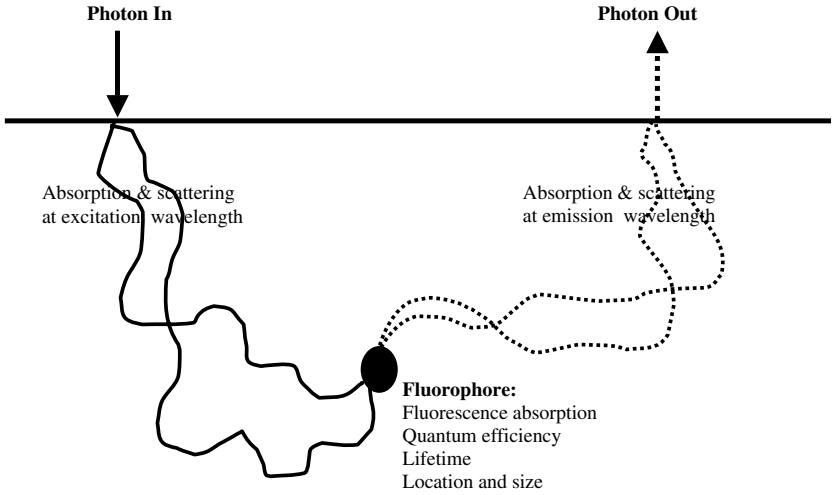

Figure 3. Scheme of diffuse fluorescence photon migration inside turbid medium.

The phantom was approximately 0.6 mm length of fluorescent dye (Molecular Probes Far Red Fluosphere latex, excitation/emission = 690/720, concentration 2% by volume) in a glass capillary of ID 0.5 mm. In all measurements the camera and laser remained focused at the surface of the medium. In this study only one fluorescent target was placed inside the turbid medium.

In the first set of experiments, a container filled with Intralipid solution (Baxter 20%, diluted to 1% with distilled water) was used to simulate a tissue-like medium. The capillary tube containing the dye was attached to a three-axis micrometer translation stage to allow it to be positioned precisely both in the plane of the liquid surface, as well as to adjust the depth.

The second series of experiments used *ex vivo* porcine tissue. The experimental geometry was altered slightly from that shown in figure 1 since a simple micrometer could not be used to change the depth in the solid tissue. Instead, the phantom was placed on a thick slab of the tissue serving as the infinite medium. The beam was positioned in the plane directly onto the phantom, then another slab of tissue was placed on top (the thickness of the slab is the depth of the phantom), and the camera and beam were focused on the top of this new slab by adjusting the vertical adjustment. Any depth could be simulated by the addition of more tissue slabs.

It should be noted that in many studies, aimed at the fluorescent contrast agent development, a different illumination set-up has been chosen, i.e. the plane wave illumination. This scheme was able to provide undistorted 2D maps of the fluorescent agent distribution in the small animal studies without an additional data processing (see e.g. Zaheer *et al* (2001) and Bugaj *et al* (2001)). For 3D fluorophore localization presented in this paper, we have used a 'point source' illumination that is usually applied in the optical tomographic studies (e.g. Lee and Sevick-Muraca (2002) and Ntziachristos and Weissleder (2001)).

3. Theoretical model and reconstruction algorithm

Figure 3 illustrates light propagation in the turbid medium for the considered experimental setup. An incident photon, after several scattering events, reaches and excites the embedded fluorophore and, after a time delay (the fluorescence lifetime), is reemitted at the fluorescence

wavelength with some quantum efficiency. That emitted photon travels to the detector, again experiencing scattering inside the turbid medium. Absorption of both incident and emitted light influences the measured intensities as well. Thus, the optical parameters of the medium important for analysis of the photon migration in experiments with deeply embedded fluorescent markers are scattering and absorption coefficients at incident and emitted wavelengths: μ_{si}, μ_{ai}, μ_{se} and μ_{ae}, respectively.

The forward model, describing photon migration for the CW case in the reflectance mode, was found recently from the random walk theory (Gandjbakhche and Gannot 1996, Gandjbakhche *et al* 1997) , which represents photons as random walkers moving isotropically between neighbouring points of the cubic lattice with spacing $(\mu_s')^{-1}$, where $\mu_s' = \mu_s(1-g)$ is the transport-corrected scattering coefficient, and g is a usual scatter anisotropy factor. The measured intensity of emitted light is proportional to the probability that the fluorophore absorbs the incident photon and then decays into a photon at the emission wavelength that eventually reaches the detector.

The corresponding theoretical expression for this probability is rather complicated (Gandjbakhche *et al* 1997, Chernomordik *et al* 1999):

$$\Gamma(\mathbf{r},\mathbf{s}) = \frac{\Phi\frac{\mu_{af}}{\mu_{sf}'}\left[H(\alpha_-,\beta_-) - H(\alpha_-,\beta_+) - H(\alpha_+,\beta_-) + H(\alpha_+,\beta_+)\right]\exp\left(-\frac{\mu_{ae}}{\mu_{se}'}\right)}{\left\{1 - \frac{\mu_{af}}{\mu_{sf}'} + \frac{\mu_{af}}{\mu_{sf}'}\left[1 + \frac{1}{8}\left(\frac{3}{\pi}\right)^{\frac{3}{2}}\sum_{m=1}^{\infty}\frac{1}{m^{3/2}}\exp\left(-2m\frac{\mu_{ai}}{\mu_{si}'}\right)\right]\right\}} \tag{1}$$

where

$$H(\alpha,\beta) = \frac{1}{\sqrt{\alpha\beta}}\exp\left\{-2\left[\sqrt{\alpha\frac{\mu_{ai}}{\mu_{si}'}} + \sqrt{\beta\frac{\mu_{ae}}{\mu_{se}'}}\right]\right\} \tag{2}$$

$$\alpha_\pm = \frac{3}{4}\left[\bar{x}_f^2 + \bar{y}_f^2 + \left(\bar{z}_f \pm \frac{\sqrt{2}}{\mu_{si}'}\right)^2\right]{\mu_{si}'}^2$$

and

$$\beta_\pm = \frac{3}{4}\left[(\bar{x}_f - \bar{x})^2 + (\bar{y}_f - \bar{y})^2 + \left(\bar{z}_f + \frac{\sqrt{2}}{\mu_{se}'} \pm \frac{\sqrt{2}}{\mu_{se}'}\right)^2\right]\mu_{se}'.$$

We have chosen an *XYZ* coordinate system with a *Z*-axis perpendicular to the surface of the medium. Therefore, *Z*-value corresponds to the target depth. Lateral shift (in *XY* plane) between the fluorophore position and the illumination spot, the so-called offset (see figure 1) has been varied. Due to axial symmetry results depend only on the magnitude of this shift, and not on its direction. For the sake of convenience, we assume that this lateral shift (offset) was always realized in the *X*-direction.

It is assumed here that the entry point for the incident photon is the origin of the coordinate system (0,0,0), the fluorescent site is at $(\bar{x}_f, \bar{y}_f, \bar{z}_f)$, the detector is at $(\bar{x}, \bar{y}, \bar{z})$, and $z_0 = \sqrt{2}(\mu_s')^{-1}$. The optical parameters in this equation, μ_s' and μ_a, are the transport-corrected scattering coefficient and absorption coefficient of the background. The subscripts *i* and *e* stand for incident and emitted light, and μ_{sf}' and μ_{af} are the optical characteristics of the fluorescent site. The parameter Φ is the probability that an excited fluorophore will in fact emit a fluorescent photon, i.e. it is a quantum efficiency. Parameters Φ, μ_{sf}' and μ_{af} play little role in the reconstruction, which works with the normalized intensities. The infinite sum in the denominator of the RHS of equation (1) converges very quickly and, in principle, taking into account only the first 3–4 terms provides sufficient accuracy for an intensity estimate (Gandjbakhche *et al* 1997). For a suggested reconstruction method, however, the effect of

this summation can be neglected altogether since it does not change the normalized intensity distributions used in the presented approach.

The inverse algorithm is based on a multi-parameter curve fitting procedure, written in C++ as a standard Levenberg–Marquardt procedure (Press *et al* 1992). It uses the theoretical expression for diffuse fluorescent intensity (CW case), obtained from the random walk theory as a forward model (equation (1)) (Chernomordik *et al* 1999). The problem can be easily reduced from 2D to 1D for a given field of view of the detector (e.g. a CCD camera) by introducing a single variable that characterizes the position of the pixel in the image plane $w = (x/s)n_{sc} + y/s$. Here s is the distance between neighbouring pixels, and $n_{sc}$is the number of pixels in each linear scan ($n_{sc} = 512$ for our square image field of 512×512 pixels). The field-of-view of our measurement system—in other words the physical dimensions of the corresponding surface area of the sample—was 50×50 mm. This field-of-view did not depend on the excitation light coverage (which corresponds to a single pixel for our experimental setup), since the sensitivity and/or integration time of our CCD camera was sufficient to detect the emitted light all over the image field.

As mentioned above, in this case the analysis was limited to a single fluorophore in the field-of-view. If there proved to be several fluorophores in the original field-of-view (which would be likely when imaging sentinel lymph nodes), we suggest a straightforward strategy of image analysis, based on dividing the field-of-view into several domains (regions of interest), each containing not more than two fluorophores) and their sequential analysis.

It should be noted that for several fluorescent sites, the detected signal could be considered as a sum of signals from individual fluorophores. As was shown before (Chernomordik *et al* 1999), this assumption works well for tissue-like phantoms with two embedded fluorophores within the field of view, and the reconstruction algorithm, based on the random walk model, is capable of localizing their positions and relative strengths (i.e. amount of the fluorescent contrast agent).

For the case of one embedded fluorophore, the fitting parameters are the coordinates of the fluorophore in question and the background intensity. Values considered to be known *a priori* are the field-of-view dimensions (i.e. number of pixels along each axis) and inter-pixel distance (scanning step). To start the reconstruction, initial values of the background optical parameters (μ'_{si}, μ_{ai}, μ'_{se}, μ_{ae} at excitation and emission wavelengths) are chosen. This choice can be based on data from literature and verified by the calibration, using measurements of total reflectance and transmittance by the method of integrating spheres (see e.g. Gannot *et al* (1998)). We can either keep these optical parameters (except, μ'_{si}) fixed in our iteration process or let them vary—the estimated values of the fluorophore depth proves to be very close to the nominal values (see also Chernomordik *et al* (1999)).

Our analysis shows the shape of the intensity distribution of the emitted light is considerably more sensitive to the depth of the fluorophore than to the influence of the optical parameters (scattering and absorption coefficients) of the background medium. This fact improves the robustness of the algorithm since these parameters are difficult to measure. In fact, we could add three of the four optical characteristics of the medium (except for μ'_{si} which is needed for scaling the distances) to the list of fitting parameters without major improvement in the estimated fluorophore depth.

Equation (1) predicts strong dependence of the width of the intensity distribution on the depth of the fluorophore as is illustrated by figure 4(a), where predicted cross-sections through the maximum are presented for $z_f = 2, 4, 8$ and 16 mm. Such behaviour was observed in our experimental data. It should be noted that for a given fluorophore depth the width of the fluorescent intensity distribution is determined by the scattering and absorption coefficients of the medium. As an example of expected influence of the optical parameters of the medium

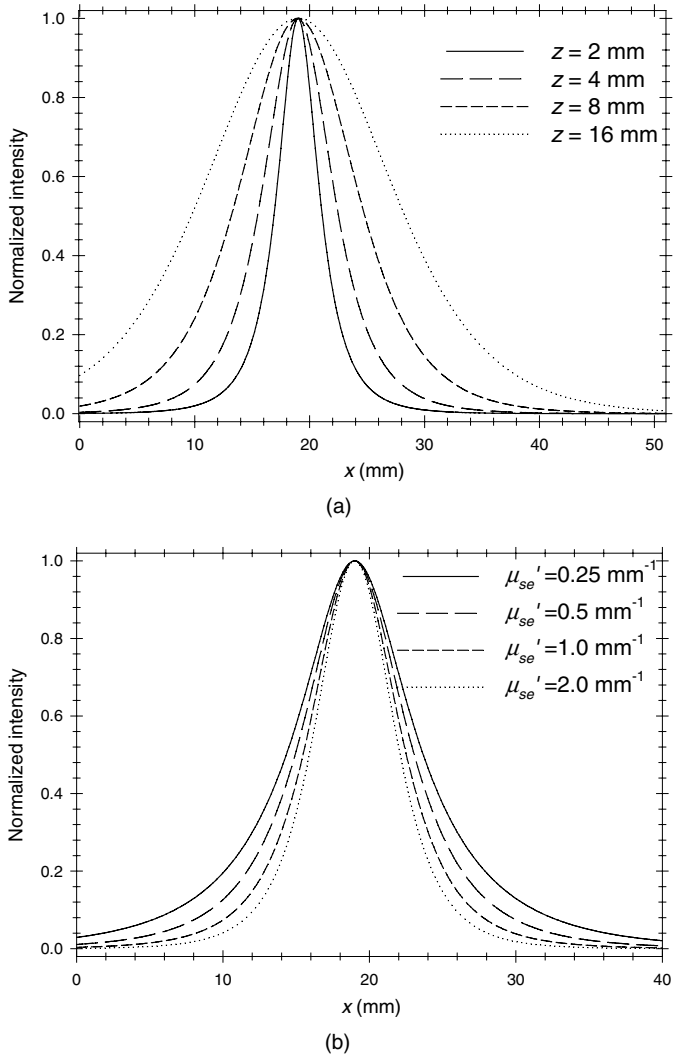

Figure 4. (a) Lateral distribution of the fluorescent intensity as a function of the fluorophore depth, expected from the theoretical model. (b) Lateral distribution of the fluorescent intensity as a function of the scattering coefficient of the background at emission wavelength, expected from the theoretical model.

on the shape of the normalized intensity distribution, an effect of variation in scattering is illustrated by figure 4(b) where the scattering coefficient was changed over an eight-fold range. Though some changes in distributions are observed, they are minor, comparing with the major changes resulted from an eight-fold change in the fluorophore depths presented in figure 4(a). Similar situation for the case of scattering variation is expected with the intensity shape changes due to variation in the absorption coefficient of the medium. Variation of the dye concentration inside the capillary should not result in the changes of the shape of the normalized intensity, as long as the fluorophore can be considered a point-like source. To avoid possible misunderstanding, though it is not important for our algorithm, based on analysis of the normalized intensity distributions, it should be emphasized that both optical

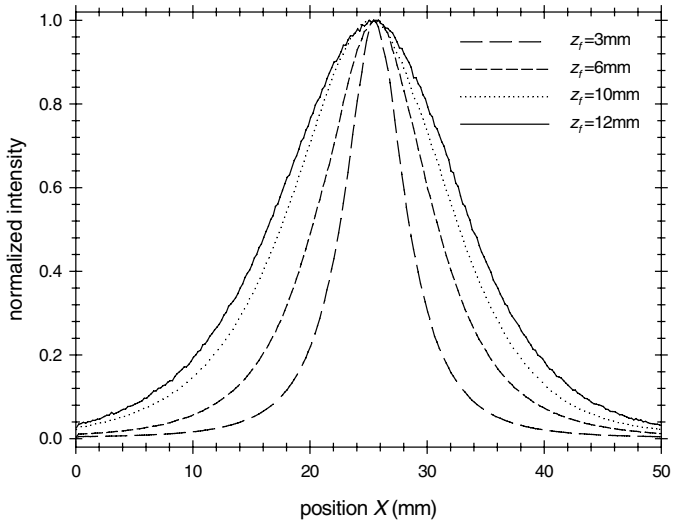

Figure 5. Experimental lateral distribution of the fluorescent intensity as a function of the fluorophore depth.

parameters of the medium and the dye concentration have strong effect on the intensity level, e.g. maximum observed intensity.

4. Results

Figure 5 shows a series of single row cross-sections for phantom depths $z_f = 4, 6, 10$ and 12 mm, with the origin defined to be directly below the laser. Each cross-section was normalized to the maximum value in the image and passes through the intensity maximum. Note the strong effect of the target depth on the width of the emitted intensity distribution. In this figure, experimental dependencies of the normalized distributions are presented. These cross-sections were obtained for the Intralipid medium with a zero lateral offset between the laser and the fluorophore. For the case of one fluorophore at varying depths in the region of interest, however, the shape of these distributions does not depend on the lateral offset d_0, as illustrated by figure 6. Only the magnitude of the maximum intensity decreases with increasing d_0 in accordance with the decrease of the intensity of the incident light near the target.

Figures 7(a) and (b) show the results of the curve fitting procedure in the form of intensity cross-sections, passing through the maximum, for the phantom in Intralipid at depths $z_f = 3.0$ and 12.0 mm, respectively. Agreement between the theoretical model and experimental data is very good. It is not surprising that the lateral coordinates of the fluorescent site close to the point of maximum intensity of the image are estimated with very good accuracy (error $\leqslant 1$ mm).

The small deviation between theory and experiment at $Y = 25$ shown in figure 7(b) is due to the excitation laser beam leaking through the emission filter. The position coincides with the position of the incident laser beam on the sample surface, since the excitation light flux is always greatest directly above the incident spot (due to specular reflection off the liquid surface). In spite of the extremely small ratio of the fluorescent signal to the reflected incident light signal, the aforementioned deviation was observed in only one experiment with an Intralipid phantom, and that was when the fluorophore was placed at the largest analysed distance from the incident spot (depth $z_f = 12$ mm and offset $d_0 = 8$ mm). This shows that

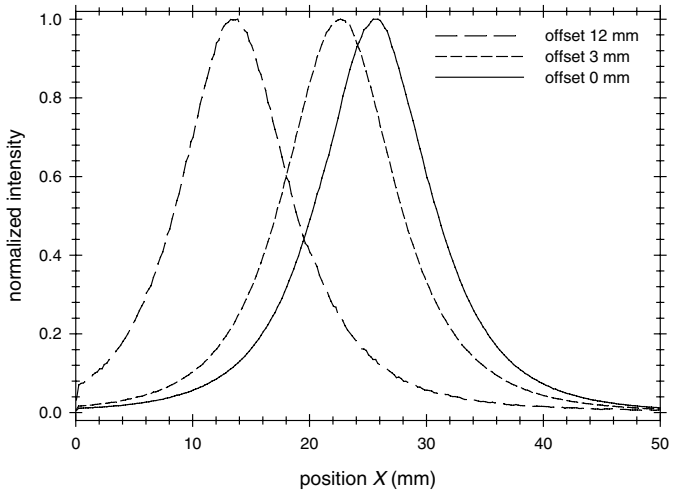

Figure 6. Experimental lateral distribution of the fluorescent intensity as a function of the offset between the source and the fluorophore position.

for our experimental conditions, the spectral filter, described in section 2, was quite effective in excluding the excitation light from the detector.

Table 1 presents the actual versus predicted depths for nine randomly selected depths and offsets. The most important fact is that the depth of the fluorophore is predicted to an error $\leqslant 10\%$, as is illustrated by the last column of the table 1. It is worth noting that the smallest relative errors (except for case V) were observed for the fluorophores at the intermediate depths $z_f = 6$–10 mm of the observed range. The reason for this is not clear at this moment. The theoretical model seems quite adequate for the observed range of depths. Perhaps at smaller depths the narrower widths of the intensity distributions do not provide optimal conditions for the accurate reconstruction due to smaller number of the image pixels that contain useful information about the emitted light. On the other hand, at greater depths, to achieve an optimal reconstruction we should increase the field of view for better presentation of the tails of the observed distribution.

The reconstructed depths for the experiments using the *ex vivo* porcine tissue slabs were also quite promising. Examples of the raw 2D images of the fluorophores at different depths inside *ex vivo* tissue slabs are presented in figures 8(a) and (b). Both images are normalized to the brightest pixel in the image. As expected (see figure 4(a)), the deeper the fluorophore, the broader the bright spot on the image plane. Although the intensity distributions were not as smooth as for the Intralipid case due to the inhomogeneous nature of the medium, we were able to estimate the fluorophore positions at different depths (5.28, 11.5 mm) with error $\leqslant 15\%$. Corresponding examples of intensity single CCD row cross-sections are presented in figures 9(a) and (b), and the comparison of the experimental and predicted values are presented in table 2.

5. Summary and future directions

Our purpose is to develop a technique for *in vivo* detection of exogenous fluorescent markers inside sentinel nodes and reconstruction of their depths. We have designed a highly sensitive near-infrared laser imaging system that can be used in combination with a reconstruction

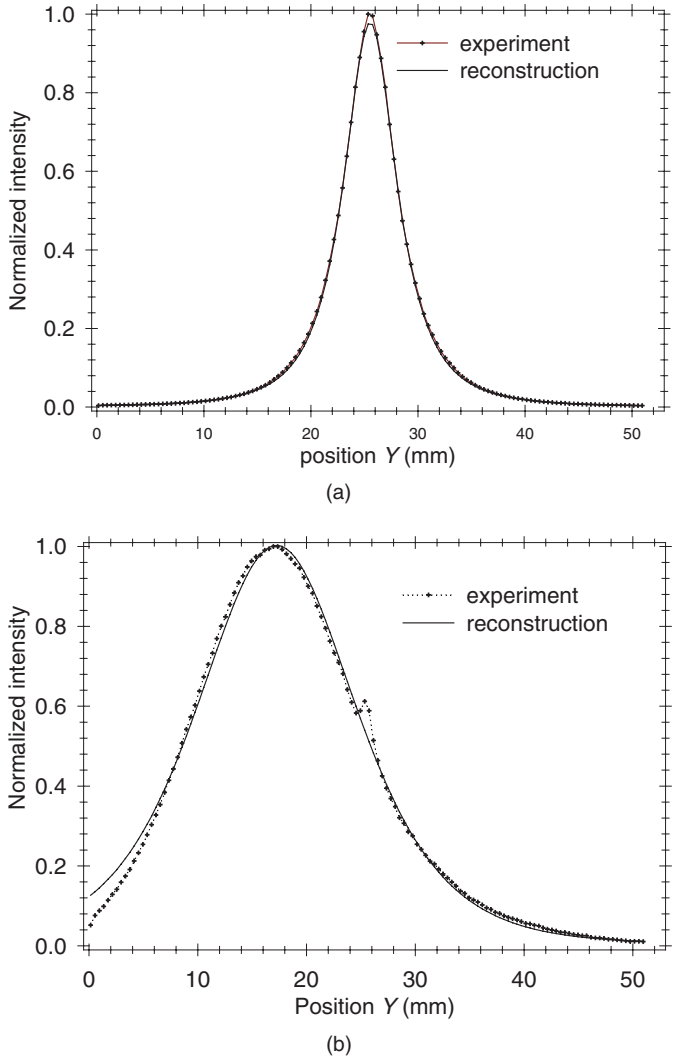

Figure 7. Emitted intensity single row cross sections (one fluorophore at different depths inside Intralipid solution): experimental data versus reconstructed theoretical curves $z_f = 3$ mm, $z_f = 12$ mm.

algorithm—based on the random walk theory—to estimate 3D positions of fluorescent masses from the obtained surface images. The results of the reconstruction for both the Intralipid and *ex vivo* tissue are encouraging. The small deviation seen in one experiment was due to reflected excitation light leaking through the filter, and implies that expanding our methodology for larger fluorophore depths and offsets would require use of even more selective filters.

From an experimental point of view, the next important step in realizing our goal is to develop fluorescent beads that can be injected into the tumour bed and then carried by lymphatics to the corresponding sentinel node(s) (Hawley *et al* 1997a, 1997b, Moghimi *et al* 1994) for imaging. We also will investigate the contribution of the size of the imaged structure,

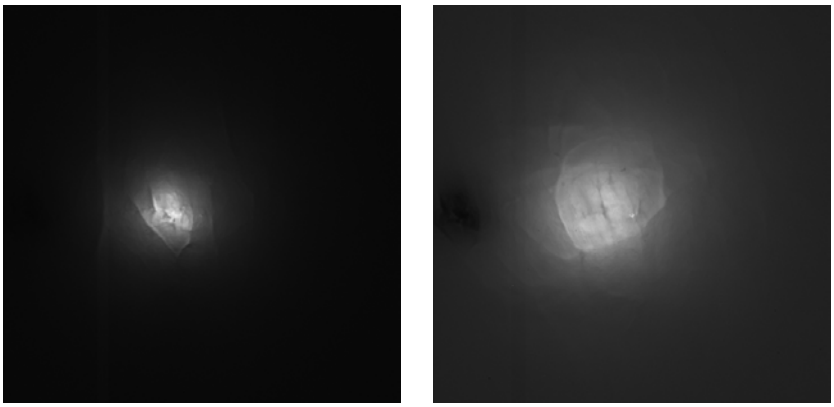

Figure 8. 2D images of the fluorophores at different depths inside *ex vivo* tissue slabs $z_f = 5.28$ mm, $z_f = 11.50$ mm.

Table 1. Comparison of the predicted fluorophore depths with experimental values (single target inside Intralipid solution).

Experiment	Offset (mm)	Actual depth (mm)	Predicted depth (mm)	Error (%)
I	0	6.0	6.20	3.33
II	0	3.0	2.87	−4.33
III	6	12.0	11.49	−4.25
IV	8	2.0	1.92	−4.00
V	12	2.0	1.97	−1.50
VI	3	6.0	6.20	3.33
VII	8	12.0	11.30	−5.83
VIII	0	10.0	10.14	1.40
IX	12	6.0	6.09	1.50

Table 2. Comparison of the predicted fluorophore depths with actual values (single target inside *ex vivo* porcine tissue slab).

Experiment	Offset (mm)	Actual depth (mm)	Predicted depth (mm)	Error (%)
I	0	5.28	4.50	15.0
II	4	5.28	4.70	11.0
IV	8	5.28	4.87	7.8
V	12	5.28	4.98	5.7
VI	0	11.50	10.27	10.7
VII	4	11.50	10.21	11.2
VIII	8	11.50	11.25	2.2

the type of near-infrared dye to maximize intensity for localization, and the contribution of varying host tissue structure such as skin, muscle and fat.

Optically guided biopsies will be able to supplant the use of radioactivity-based methods currently being used. Given that the vast majority of the 186 000 cases of breast cancer each year in the USA undergo node interrogation, the fluorescent-guided biopsying would provide a safe and efficient platform for diagnosis and prognosis.

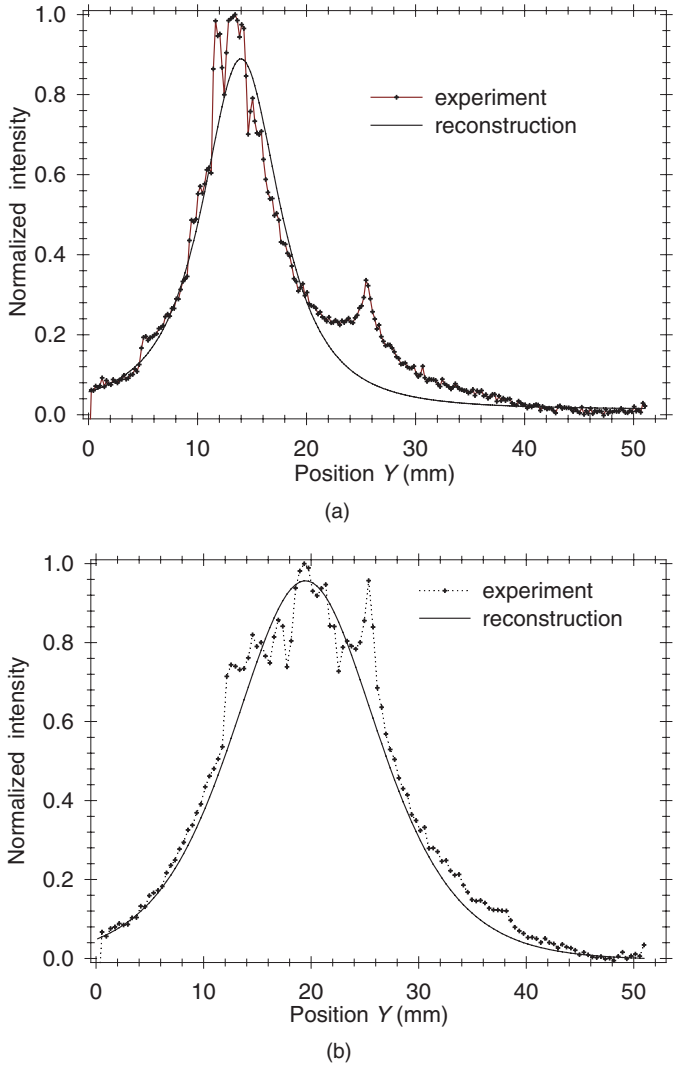

Figure 9. Emitted intensity single row cross sections (one fluorophore at different depths inside *ex vivo* tissue slab): experimental data versus reconstructed theoretical curves $z_f = 5.28$ mm, $z_f = 11.50$ mm.

References

Bugaj J E, Achilefu S, Dorshow R B and Rajagopalan R 2001 Novel fluorescent contrast agents for optical imaging of *in vivo* tumors based on a receptor-targeted dye-peptide conjugate platform *J. Biomed. Opt.* **6** 122

Chernomordik V, Hattery D, Gannot I and Gandjbakhche A H 1999 Inverse method 3-D reconstruction of localized *in vivo* fluorescence—application to Sjogren syndrome *IEEE J. Sel. Top. Quantum Electron.* **5** 930

Cox C E *et al* 2000 Lymphatic mapping and sentinel lymph node biopsy in patients with breast cancer *Annu. Rev. Med.* **51** 525

Eppstein M J, Dougherty D E, Hawrysz D J and Sevick-Muraca E M 2001 Three-dimensional Bayesian optical image reconstruction with domain decomposition *IEEE Trans. Med. Imaging* **20** 147

Gandjbakhche A H, Bonner R F, Nossal R and Weiss G H 1997 Effects of multiple-passage probabilities on fluorescent signals from biological media *Appl. Opt.* **36** 4613

Gandjbakhche A H and Gannot I 1996 Quantitative fluorescent imaging of specific markers of diseased tissue *IEEE J. Sel. Top. Quantum Electron.* **2** 914

Gannot I, Bonner R F, Gannot G, Fox P C, Smith P D and Gandjbakhche A H 1998 Optical simulations of a noninvasive technique for the diagnosis of diseased salivary glands *in situ Med. Phys.* **25** 1139

Glass E C, Essner R and Giuliano A E 1999 Sentinel node localization in breast cancer *Semin. Nucl. Med.* **29** 57

Hawley A E, Illum L and Davis S S 1997a Lymph node localisation of biodegradable nanospheres surface modified with poloxamer and poloxamine block co-polymers *FEBS Lett.* **400** 319

Hawley A E, Illum L and Davis S S 1997b Preparation of biodegradable, surface engineered PLGA nanospheres with enhanced lymphatic drainage and lymph node uptake *Pharm. Res.* **14** 657

Hawrysz D J, Eppstein M J, Lee J W and Sevick-Muraca E M 2001 Error consideration in contrast-enhanced three-dimensional optical tomography *Opt. Lett.* **26** 704

Hawrysz D J and Sevick-Muraca E M 2000 Developments toward diagnostic breast cancer imaging using near-infrared optical measurements and fluorescent contrast agents *Neoplasia* **2** 388

Lee J and Sevick-Muraca E M 2002 Three-dimensional fluorescence enhanced optical tomography using referenced frequency-domain photon migration measurements at emission and excitation wavelengths *J. Opt. Soc. Am.* A **19** 759

Li X D, OLeary M A, Boas D A, Chance B and Yodh A G 1996 Fluorescent diffuse photon: density waves in homogeneous and heterogeneous turbid media: analytic solutions and applications *Appl. Opt.* **35** 3746

Moghimi S M, Hawley A E, Christy N M, Gray T, Illum L and Davis S S 1994 Surface engineered nanospheres with enhanced drainage into lymphatics and uptake by macrophages of the regional lymph- nodes *FEBS Lett.* **344** 25

Ntziachristos V and Weissleder R 2001 Experimental three-dimensional fluorescence reconstruction of diffuse media by use of a normalized Born approximation *Opt. Lett.* **26** 893

Patterson M S and Pogue B W 1994 Mathematical-model for time-resolved and frequency-domain fluorescence spectroscopy in biological tissue *Appl. Opt.* **33** 1963

Press W H, Teukolsky S A, Vetterling W T and Flannery B P 1992 *Numerical Recipes in C: The Art of Scientific Computing* (Cambridge: Cambridge University Press)

Reynolds J S, Troy T L, Mayer R H, Thompson A B, Waters D J, Cornell K K, Snyder P W and Sevick-Muraca E M 1999 Imaging of spontaneous canine mammary tumors using fluorescent contrast agents *Photochem. Photobiol.* **70** 87

Roy R and Sevick-Muraca E M 2001 Three-dimensional unconstrained and constrained image- reconstruction techniques applied to fluorescence, frequency- domain photon migration *Appl. Opt.* **40** 2206

van Dongen J A, Voogd A C, Fentiman I S, Legrand C, Sylvester R J, Tong D, van der Schueren E, Helle P A, van Zijl K and Bartelink H 2000 Long-term results of a randomized trial comparing breast- conserving therapy with mastectomy: European Organization for Research and Treatment of Cancer 10801 trial *J. Natl. Cancer Inst.* **92** 1143

Wagnieres G A, Star W M and Wilson B C 1998 *In vivo* fluorescence spectroscopy and imaging for oncological applications *Photochem. Photobiol.* **68** 603

Weissleder R 2002 Scaling down imaging: molecular mapping of cancer in mice *Nature Reviews Cancer* **2** 11

Zaheer A, Lenkinski R E, Mahmood A, Jones A G, Cantley L C and Frangioni J V 2001 In vivo near-infrared fluorescence imaging of osteoblastic activity *Nat. Biotechnol.* **19** 1148